Robust RF Fingerprinting Under Power Amplifier Variations via Joint Nonlinearity and Channel Modeling

Shiqi Zhang, *Graduate Student Member, IEEE,* Aiqun Hu, *Senior Member, IEEE,* Hua Fu, *Member, IEEE,* and Zhen Zhang

***Abstract*—Radio Frequency Fingerprinting (RFF) methods exploiting power amplifier (PA) nonlinearities suffer in practice from hardware variations, power control mechanisms and multipath channel distortions. To overcome these limitations, we introduce a unified system model that simultaneously captures PA-induced nonlinear behaviors and wireless channel convolution effects. Building on this model, we design a Half-Quadratic Splitting (HQS) alternating optimization that successively disentangles and estimates the channel matrix and PA nonlinear coefficients. To further regularize coefficient recovery, we integrate a Deep Signal Prior (DSP) implemented as an untrained 1D U-Net with Total Variation loss. Evaluations on real-world LoRa datasets demonstrate that the proposed method achieves robust identification, attaining 96.80% accuracy under line-of-sight and 91.19% under non-line-of-sight conditions, even across unseen PA modules and varying power levels.**

***Index Terms*—Radio Frequency Fingerprinting, Power Amplifier, Nonlinear**

I. Introduction

THE rapid development of the Internet of Things (IoT) has significantly increased the demand for reliable and secure wireless communication, particularly in addressing identification challenges arising from the inherent openness of wireless channels [1]. RFF, which leverages the intrinsic hardware imperfections of wireless transmitters, has emerged as a promising technique for device identification at the physical layer to enhance IoT security [2]. These hardware-induced features originate from various RF components, such as in-phase and quadrature (I/Q) imbalance introduced by mixers [3], frequency offset caused by oscillators [4], and nonlinear distortion contributed by PA [5]–[10].

PAs are widely deployed in RF front-end systems to boost transmit power, but they inherently introduce nonlinear distortions into the transmitted signals. Moreover, variations in PA characteristics can significantly alter the RFF features of a device. As a result, extensive research has focused on exploiting PA-induced nonlinearity for device identification. For instance, [6] addressed the difficulty of distinguishing devices using identical PA models under low-to-moderate SNR conditions by leveraging Physical Unclonable Functions (PUFs) to fine-tune PA nonlinear characteristics and amplify RFF diversity. In [7], the authors proposed using the nonlinear memory effects generated by cascading a nonlinear PA with preceding and succeeding root raised cosine (RRC) filters, exploiting the induced inter-symbol interference (ISI) as discriminative RFF features. In [8], the PA was partitioned into independently switchable transistor slices, enabling the dynamic generation of up to 220 distinct RFF signatures on the same device through combinatorial randomness.

However, in practical deployment scenarios, PA-based RFF techniques face several challenges. First, due to varying operational requirements, IoT devices may replace or augment their transmission chains with different PA modules. For example, some LoRa devices may add external PA units to adapt to changes in transmission distance, resulting in a mismatch between the original RFF and the current hardware configuration, thereby degrading identification accuracy. Second, uplink power control mechanisms [11] may dynamically adjust PA output power levels, while most existing studies [6] [7] are conducted under fixed PA settings, limiting generalization. Third, wireless channel impairments can significantly distort nonlinear RFF features [9]. Efforts to mitigate channel effects have been proposed. In [9], channel compensation was performed by estimating mixed coefficients of PA nonlinearity and the channel, followed by division using different sequence lengths. However, the channel model adopted remains relatively simplistic. In [10], robust RFF features were obtained by dividing short-time Fourier transforms (STFT) of high and low power transmissions to suppress channel and noise effects, although the identification procedure becomes substantially more complex.

Despite these advances, to the best of our knowledge, no prior work has explicitly addressed the problem of intentionally compensating for PA-induced nonlinearity to isolate stable residual device fingerprints, thereby enabling robust identification across amplifier changes, power control variations, and channel dynamics. The main contributions of this work are summarized as follows:

- A unified system model is established that jointly characterizes the nonlinear behavior of power amplifiers (PAs) and the wireless channel convolution effects, providing a principled basis for robust fingerprint extraction in realistic IoT environments.
- A Half Quadratic Splitting (HQS)-based alternating optimization framework is developed to decouple and iteratively estimate the unknown channel matrix and the nonlinear coefficients, where the channel estimation employs a set of regularization factors to enhance robustness under varying SNR conditions. Inspired by [12], a deep signal prior (DSP) strategy is incorporated by modeling the nonlinear coefficients as the output of an untrained

Corresponding author: Aiqun Hu.

Shiqi Zhang and Aiqun Hu are with the National Mobile Communications Research Laboratory, Southeast University, Nanjing 210096, China (e-mail: zhangshq@seu.edu.cn; aqhu@seu.edu.cn).

Hua Fu and Zhen Zhang are with the School of Cyber Science and Engineering, Southeast University, Nanjing 211189, China (e-mail: hfu@seu.edu.cn; z_zhang@seu.edu.cn).

lightweight 1D U-Net, leveraging the implicit structural prior without requiring labeled ground truth.
- Extensive experiments are conducted on a custom-collected LoRa device dataset under practical deployment variations, including amplifier switching, power control, and channel conditions. The results demonstrate the effectiveness of the proposed method in achieving stable device identification across hardware and channel variations.

The rest of the paper is organized as follows. Section II introduces the joint system model that accounts for both PA nonlinearity and channel convolution and the HQS-based alternating optimization framework. Section III details the experimental setup and evaluation results. Finally, Section IV concludes the paper.

II. System Model

A. Power Amplifier Model

We consider a polynomial model to characterize the nonlinear behavior of the power amplifier (PA) at baseband. The discrete-time output signal $x[n]$ is expressed as:

$$x[n] = \sum_{k=0}^{K} a_{2k+1}\, d[n]\, \big|d[n]\big|^{2k}, \tag{1}$$

where $d[n]$ denotes the input to the PA, i.e., the baseband signal containing RFF. The coefficients a_{2k+1} capture the odd-order nonlinear effects of the PA, while even-order terms are suppressed by the receiver's bandpass filter.

Let the input signal length be N,

$$\mathbf{x} = \mathbf{D}_N \mathbf{a}, \tag{2}$$

where $\mathbf{D}_N \in \mathbb{C}^{N\times(K+1)}$ is the design matrix whose entries are defined by:

$$\mathbf{D}_N(n,k) = d[n]\cdot|d[n]|^{2k}, \quad 0\le k\le K,\ 1\le n\le N. \tag{3}$$

$$\mathbf{a} = [a_1,\ a_3,\ \ldots,\ a_{2K+1}]^T. \tag{4}$$

B. Received Signal Model

After synchronization and downconversion at the receiver, the baseband equivalent received signal is modeled as:

$$y[n] = \sum_{\ell=1}^{L_h} h_\ell\, x[n-\ell] + \boldsymbol{\epsilon}[n], \tag{5}$$

where h_ℓ denotes the discrete-time channel impulse response of length L_h, and $\boldsymbol{\epsilon}$ is additive complex Gaussian noise. In matrix form:

$$\mathbf{y} = \mathbf{H}\mathbf{x} + \boldsymbol{\epsilon}, \tag{6}$$

where $\mathbf{y} \in \mathbb{C}^{(N+L_h-1)\times 1}$, $\mathbf{H} \in \mathbb{C}^{(N+L_h-1)\times N}$, and $\boldsymbol{\epsilon} \in \mathbb{C}^{(N+L_h-1)\times 1}$. The channel matrix $\mathbf{H}$ is a Toeplitz matrix:

$$\mathbf{H}(n,m) = \begin{cases} h_{n-m+1}, & 1\le m\le n\le N+L_h-1,\\ & 1\le n-m+1\le L_h \\ 0, & \text{otherwise} \end{cases} \tag{7}$$

By substituting Eq. (2) into Eq. (6), we obtain:

$$\mathbf{y} = \mathbf{H}\mathbf{D}_N\mathbf{a} + \boldsymbol{\epsilon}. \tag{8}$$

The received signal is then reformulated as:

$$\mathbf{y} = \mathbf{D}_N^{(L_h-1)}\hat{\mathbf{H}}\mathbf{a} + \boldsymbol{\epsilon}, \tag{9}$$

where $\mathbf{D}_N^{(L_h-1)} \in \mathbb{C}^{(N+L_h-1)\times(K+1)L_h}$ Under the assumption of short-term channel stationarity, we approximate $\hat{\mathbf{H}}$ as a block-stacked structure:

$$\hat{\mathbf{H}} = \begin{bmatrix} \mathrm{diag}(h_1) \\ \mathrm{diag}(h_2) \\ \vdots \\ \mathrm{diag}(h_{L_h}) \end{bmatrix} \in \mathbb{C}^{(K+1)L_h\times(K+1)}, \tag{10}$$

where each $\mathrm{diag}(h_\ell) \in \mathbb{C}^{(K+1)\times(K+1)}$ is a diagonal matrix with scalar tap h_ℓ applied uniformly to each nonlinear order term.

$\mathbf{D}_N^{(L_h-1)}$ is constructed as:

$$\mathbf{D}_N^{(L_h-1)} = \left[\mathbf{D}_N^{(0)}\middle|\mathbf{D}_N^{(1)}\middle|\ldots\middle|\mathbf{D}_N^{(L_h-1)}\right], \tag{11}$$

with blocks $\mathbf{D}_N^{(m)} \in \mathbb{C}^{(N+L_h-1)\times(K+1)}$ and elements:

$$\mathbf{D}_N^{(m)}(n,k) = d[n-m]\,|d[n-m]|^{2k}, \quad 0\le m<L_h,\ 0\le k\le K. \tag{12}$$

C. Joint Modeling of $\hat{\mathbf{H}}$ and $\mathbf{a}$

Starting from the known received signal $\mathbf{y}$ and the design matrix $\mathbf{D}_N^{(L_h-1)}$, we consider the model in Eq. (9). As shown in Fig. 1, this section aims to describe in detail how to estimate the nonlinear coefficient vector $\mathbf{a}$ under unknown channel conditions.

1) Channel Matrix Estimation: To avoid ambiguity, we refer to $\hat{\mathbf{H}}$ as the *channel matrix*, aligning with common terminology in communication systems. To robustly estimate the unknown channel matrix in the presence of noise $\boldsymbol{\epsilon}$, we adopt a Minimum Mean Squared Error (MMSE) criterion. Considering varying SNR conditions, we introduce multiple regularization factors $\{\lambda_j\}$ to compute a set of channel matrices $\{\hat{\mathbf{H}}^{(j)}\}$. The MMSE estimation problem is formulated as:

$$\min_{\hat{\mathbf{H}}} E\left[\left\|\mathbf{y} - \mathbf{D}_N^{(L_h-1)}\hat{\mathbf{H}}\mathbf{a}_0\right\|_2^2\right], \tag{13}$$

where $\mathbf{a}_0$ is an initial estimate of the nonlinear coefficients. The Euclidean norm measures the reconstruction error between the observation and the model output.

Expanding the expectation yields:

$$E\left[\left\|\mathbf{y} - \mathbf{D}_N^{(L_h-1)}\hat{\mathbf{H}}\mathbf{a}_0\right\|_2^2\right] \tag{14}$$

$$= E\left[\left\|\mathbf{D}_N^{(L_h-1)}\hat{\mathbf{H}}(\mathbf{a}-\mathbf{a}_0) + \boldsymbol{\epsilon}\right\|_2^2\right]. \tag{15}$$

Assuming independence between signal and noise, and that the noise has zero mean, the expectation decomposes into:

$$E\left[\left\|\mathbf{D}_N^{(L_h-1)}\hat{\mathbf{H}}(\mathbf{a}-\mathbf{a}_0)\right\|_2^2\right] + E\left[\|\boldsymbol{\epsilon}\|_2^2\right]. \tag{16}$$

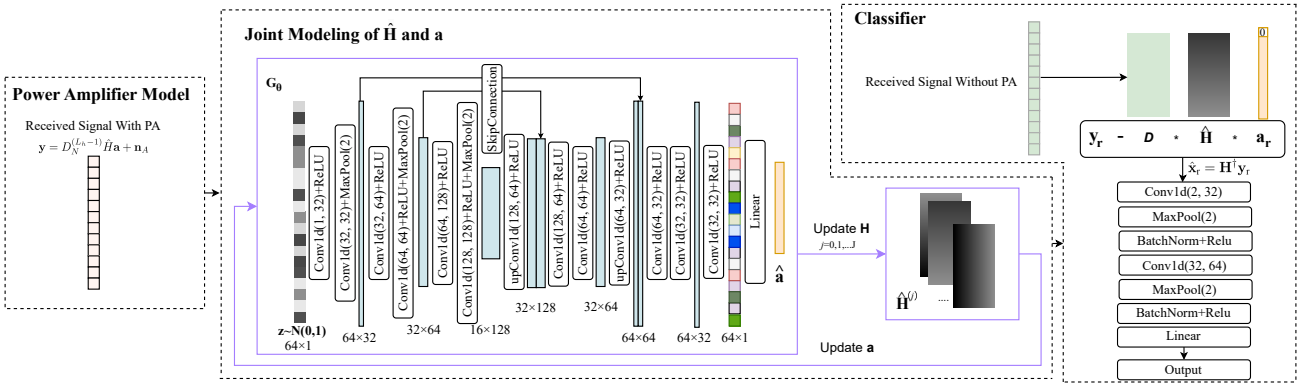

Fig. 1: Overview of the proposed joint modeling and classification framework. A fixed random Gaussian vector $z \sim \mathcal{N}(0,1)$ is passed through a 1D U-Net generator G_θ to produce the nonlinear coefficient vector $\mathbf{a}$. This coefficient is jointly estimated with the channel matrix $\hat{\mathbf{H}}^{(j)}$ under multiple SNR conditions using an alternating HQS-based optimization scheme. The nonlinear artifact, constructed as $\mathbf{D}_N^{(L_h-1)}\hat{\mathbf{H}}\mathbf{a}_\mathrm{r}$, is subtracted from the received signal $\mathbf{y}$ to obtain a linearized version $\mathbf{y}_r$. Here, the design matrix $\mathbf{D}_N^{(L_h-1)}$ is generated from signals collected without power amplifier distortion, serving as a reference. To further eliminate residual channel distortion, a Tikhonov-regularized inverse filter $\mathbf{H}^\dagger$ is applied to $\mathbf{y}_r$, yielding the equalized waveform $\hat{\mathbf{x}}_r$, which is then fed into a 1D CNN classifier for robust device identification.

Since the noise variance is assumed known, we regularize the problem by introducing a Frobenius-norm-based Tikhonov term for robustness. Thus, for each predefined regularization factor λ_j, the estimation of the corresponding channel matrix $\hat{\mathbf{H}}^{(j)}$ becomes:

$$\hat{\mathbf{H}}^{(j)} = \arg\min_{\hat{\mathbf{H}}} \left\| \mathbf{y} - \mathbf{D}_N^{(L_h-1)}\hat{\mathbf{H}}\mathbf{a}_0 \right\|_2^2 + \lambda_j \left\| \hat{\mathbf{H}} \right\|_F^2 \tag{17}$$

where λ_j is a regularization factor corresponding to the noise level, enabling robust estimation under varying SNR conditions. This multi-regularization strategy improves robustness under diverse channel and noise conditions.

2) HQS-Based Alternating Optimization: We adopt a Half Quadratic Splitting (HQS) strategy to alternately update the set of channel matrices $\{\hat{\mathbf{H}}^{(j)}\}$ and the nonlinear coefficients $\mathbf{a}$. Our objective is to minimize the following joint loss:

$$\begin{aligned} \min_{\mathbf{a},\{\hat{\mathbf{H}}^{(j)}\}} \; & \frac{1}{J}\sum_{j=1}^{J} \left\| \mathbf{y} - \mathbf{D}_N^{(L_h-1)}\hat{\mathbf{H}}^{(j)}\mathbf{a} \right\|_2^2 \\ & + \lambda_a R_a(\mathbf{a}) + \sum_{j=1}^{J} \lambda_j \left\| \hat{\mathbf{H}}^{(j)} \right\|_F^2 \end{aligned} \tag{18}$$

where $R_a(\cdot)$ denotes the prior on $\mathbf{a}$, implicitly modeled via a DSP network.

We follow an alternating minimization scheme, consisting of two steps per iteration.

Step 1: Update $\{\hat{\mathbf{H}}^{(j)}\}$. Given the current nonlinear coefficient estimate $\mathbf{a}^{(t)}$, we first solve the unconstrained Tikhonov-regularized least-squares problem:

$$\widetilde{\mathbf{H}}^{(j)} = \arg\min_{\mathbf{H}} \left\| \mathbf{y} - \mathbf{D}_N^{(L_h-1)}\mathbf{H}\mathbf{a}^{(t)} \right\|_2^2 + \lambda_j \|\mathbf{H}\|_F^2, \tag{19}$$

using vectorization and the Kronecker product identity:

$$A = \left(\mathbf{a}^{(t)}\right)^T \otimes \mathbf{D}_N^{(L_h-1)}, \tag{20}$$

$$\mathbf{h}^{(j)} = \left(A^H A + \lambda_j I\right)^{-1} A^H \mathbf{y}, \tag{21}$$

$$\widetilde{\mathbf{H}}^{(j)} = \mathrm{reshape}\left(\mathbf{h}^{(j)},\ (K+1)L_h,\ K+1\right). \tag{22}$$

To ensure physical consistency with the assumed model structure in Eq. (10), we constrain each $(K+1)\times(K+1)$ sub-block to be a scalar multiple of the identity matrix. This enforces that the same channel tap h_ℓ applies uniformly to all nonlinear terms of the same delay order.

We implement this by projecting each block $\widetilde{\mathbf{H}}_\ell^{(j)}$ onto the scalar-identity space:

$$\hat{\mathbf{H}}_\ell^{(j)} = \mathcal{P}_{\mathrm{sI}}\left(\widetilde{\mathbf{H}}_\ell^{(j)}\right) = \left(\frac{1}{K+1}\mathrm{tr}\left(\widetilde{\mathbf{H}}_\ell^{(j)}\right)\right)\cdot \mathbf{I}_{K+1}, \tag{23}$$

$$\forall \ell = 1,\ldots,L_h. \tag{24}$$

Step 2: Update $\mathbf{a}$. With all $\hat{\mathbf{H}}^{(j)}$ fixed, we introduce a generator $G_\theta(\cdot)$ to estimate $\mathbf{a}$. Inspired by the Deep Image Prior (DIP) framework, we treat $\mathbf{a}$ as the output of a convolutional network conditioned on a fixed random input z_a:

$$\min_\theta \frac{1}{J}\sum_{j=1}^{J} \left\| \mathbf{y} - \mathbf{D}_N^{(L_h-1)}\hat{\mathbf{H}}^{(j)}G_\theta(z_a) \right\|_2^2 + \lambda_a \mathrm{TV}(G_\theta(z_a)) \tag{25}$$

We refer to this approach as *DSP* (Deep Signal Prior) due to its application in the 1D signal domain. The generator G_θ is a lightweight 1D U-Net that maps the Gaussian noise vector $z_a \sim \mathcal{N}(0,1)$ to the estimated nonlinear coefficient vector:

$$\hat{\mathbf{a}}^{(t+1)} = G_{\theta^{(t)}}(z_a). \tag{26}$$

Algorithm 1 HQS-Based Joint Estimation of $\{\hat{\mathbf{H}}^{(j)}\}$ and $\mathbf{a}$

Input: Received signal $\mathbf{y}$, design matrix $\mathbf{D}_N^{(L_h-1)}$, initial estimate $\mathbf{a}_0$, regularization factors $\{\lambda_j\}$, λ_a, fixed noise vector z_a
Output: Estimated channel matrices $\{\hat{\mathbf{H}}^{(j)}\}$, nonlinear coefficients $\hat{\mathbf{a}}$
Initialize $\mathbf{a}^{(0)} \leftarrow \mathbf{a}_0$, set iteration counter $t \leftarrow 0$
for each $j = 1$ to J **do**
  for each $t = 1$ to N_{iter} **do**
    Update channel matrix $\hat{\mathbf{H}}^{(j)}$ by solving:

$$\arg\min_{\hat{\mathbf{H}}^{(j)}} \left\| \mathbf{y} - \mathbf{D}_N^{(L_h-1)} \hat{\mathbf{H}}^{(j)} \mathbf{a}^{(t)} \right\|_2^2 + \lambda_j \left\| \hat{\mathbf{H}}^{(j)} \right\|_F^2$$

  end for
  Update $\mathbf{a}^{(t+1)} = G_{\theta^{(t)}}(z_a)$, where $\theta^{(t)}$ minimizes:

$$\frac{1}{J} \sum_{j=1}^{J} \left\| \mathbf{y} - \mathbf{D}_N^{(L_h-1)} \hat{\mathbf{H}}^{(j)} G_\theta(z_a) \right\|_2^2 + \lambda_a \mathrm{TV}(G_\theta(z_a))$$

  $t \leftarrow t + 1$
end for
Set $\hat{\mathbf{a}} \leftarrow \mathbf{a}^{(t)}$
return $\{\hat{\mathbf{H}}^{(j)}\}, \hat{\mathbf{a}}$

To suppress high-frequency fluctuations while preserving structural characteristics, we apply Total Variation (TV) regularization:

$$\mathrm{TV}(\mathbf{a}) = \sum_{i=1}^{K} |a_{i+1} - a_i|. \tag{27}$$

The generator G_θ adopts a symmetric 1D U-Net architecture. It takes a fixed Gaussian input $z \sim \mathcal{N}(0, 1) \in \mathbb{R}^{64\times 1}$ and outputs the estimated nonlinear coefficient vector $\hat{\mathbf{a}} \in \mathbb{R}^{K+1}$.

The **encoder** consists of three stages, each with two `Conv1d` layers (kernel size = 3, padding = 1), followed by `ReLU` activation and `MaxPool1d` with stride 2, progressively reducing resolution and increasing channels from 32 to 128.

The **decoder** mirrors the encoder using `UpConv1d` (transpose convolution) and `Conv1d+ReLU` for refinement. Skip connections bridge encoder-decoder layers to preserve local structure.

A final `Conv1d(32, 32)+ReLU` layer precedes a `Linear` layer, which maps the resulting feature to $\hat{\mathbf{a}}$.

Alternating updates of $\{\hat{\mathbf{H}}^{(j)}\}$ and $\mathbf{a}$ iteratively refine the estimates, ensuring both fidelity to the observations and compliance with prior signal structure.

3) Classification: To explicitly remove PA-induced nonlinear distortions, we construct a residual coefficient vector $\mathbf{a}_\mathrm{r}$ by zeroing the linear term:

$$\mathbf{a}_\mathrm{r} = [0,\, \hat{a}_3,\, \hat{a}_5,\, \ldots,\, \hat{a}_{2K+1}]^T. \tag{28}$$

We then estimate the nonlinear artifact in the received signal and subtract it to obtain a linearized version:

$$\mathbf{y}_\mathrm{r} = \mathbf{y} - \mathbf{D}_N^{(L_h-1)} \hat{\mathbf{H}} \mathbf{a}_\mathrm{r}, \tag{29}$$

where $\hat{\mathbf{H}} = \frac{1}{J} \sum_{j=1}^{J} \hat{\mathbf{H}}^{(j)}$ is the average of all regularized channel estimates.

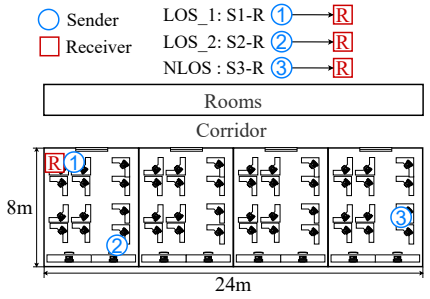

Fig. 2: Experimental setup.

To further remove residual channel distortions and obtain a clean representation for classification, we extract the Toeplitz-form baseband channel matrix $\mathbf{H} \in \mathbb{C}^{(N+L_h-1)\times N}$ by averaging the diagonal entries of each sub-block:

$$h_\ell = \frac{1}{K+1} \mathrm{tr}\left(\hat{\mathbf{H}}_\ell\right), \quad \ell = 1, \ldots, L_h, \tag{30}$$

where $\hat{\mathbf{H}}_\ell$ denotes the ℓ-th $(K+1)\times(K+1)$ diagonal block of $\hat{\mathbf{H}}$. Using $\{h_\ell\}$, we construct the channel matrix $\mathbf{H}$ as in Eq. (7). We then apply Tikhonov-regularized pseudo-inverse equalization:

$$\mathbf{H}^\dagger = \left(\mathbf{H}^H \mathbf{H} + \alpha \mathbf{I}\right)^{-1} \mathbf{H}^H, \tag{31}$$

where $\alpha > 0$. The equalized waveform is then computed as:

$$\hat{\mathbf{x}}_\mathrm{r} = \mathbf{H}^\dagger \mathbf{y}_\mathrm{r}, \tag{32}$$

which is used as the input for final classification:

$$\hat{c} = \arg\max f_\phi(\hat{\mathbf{x}}_\mathrm{r}), \tag{33}$$

where $f_\phi(\cdot)$ is a 1D CNN classifier and $\hat{c}$ denotes the predicted class label.

III. Experimental Setup

To evaluate the effectiveness and robustness of the proposed joint modeling and compensation framework, we conducted experiments using a real-world LoRa signal dataset. The experimental platform consists of ten commercial LoRa devices based on the ASR6502 chipset, operating at a carrier frequency of 433 MHz, a bandwidth of 500 kHz, a spreading factor of 10, and a sampling rate of 1 MHz. Signal reception was performed using the ADALM-Pluto SDR, which also handled synchronization.

The dataset is organized into three subsets, also shown in Fig. 2. Five different external power amplifiers (PA1–PA5) were used at the transmitter side, each with a gain ranging from 12 dB to 18 dB.

- **LOS_1 (Train):** Ten devices transmitting in a line-of-sight (LOS) environment using both **PA1** and **no PA**.
- **LOS_2 (Test):** The same ten devices in the LOS environment but using **PA2 to PA5**.
- **NLOS (Test):** Non-line-of-sight (NLOS) environment using **PA1 to PA5**.

To enhance robustness against noise and varying SNRs, we adopt a multi-regularization strategy with five values of the

regularization weight $\lambda_j \in \{0.05,\ 0.10,\ 0.15,\ 0.20,\ 0.25\}$. The order of the power amplifier model is set to $K = 3$, N_{iter} is set to 25, and λ_a is set to 0.02. We empirically tested L_h values in the range $6 \leq L_h \leq 16$, and selected $L_h = 10$ as it provided the best trade-off between performance and complexity. α in II-C3 is set to 0.001.

A. Cross-Amplifier Generalization

TABLE I: Accuracy across PA variants and environments

Method	LOS (acc%)					NLOS (acc%)	
	PA2	PA3	PA4	PA5	Avg	PA1	Other
JML+CNN	98.89	98.33	93.50	96.50	96.80	95.10	91.19
Only CNN	58.37	52.38	41.47	40.71	48.23	93.90	26.23

Table I reports the classification accuracy when the system is trained exclusively on PA1 signals and tested under both LOS and NLOS conditions across different power amplifiers (PA2–PA5). The proposed method, denoted as **JML+CNN**, where JML refers to the Joint Modeling and Learning framework described in Section II-C, consistently achieves high accuracy across all test PAs in the LOS setting, with an average accuracy of 96.80%. This demonstrates strong generalization to unseen amplifier-induced distortions. In contrast, the baseline **Only CNN**, which uses the same classifier without any compensation or preprocessing, achieves only 40.71% average accuracy in LOS and completely fails on several PA variants.

In the NLOS scenario, **JML+CNN** also maintains robust performance, achieving 95.10% accuracy on PA1 and an average of 91.19% across the remaining PA modules. By comparison, **Only CNN** drops to 26.23%, revealing its sensitivity to both channel fading and hardware variation.

B. Noise Robustness

The noise robustness of the proposed **JML+CNN** system was evaluated under varying signal-to-noise ratio (SNR) levels ranging from 35 dB to 10 dB. Fig. 3 illustrates the device identification accuracy across five test environments, including NLOS and LOS scenarios with power amplifiers PA2 through PA5. The results show that **JML+CNN** maintains consistently high performance even under low-SNR conditions. When the SNR exceeds 20 dB, the average accuracy in LOS/NLOS environments also remains above 89.26%/79.06%.

IV. Conclusion

This work has presented a unified framework for robust RF fingerprinting that jointly models PA-induced nonlinearities and multipath channel effects. By formulating the received signal as a composite of a polynomial PA model and a Toeplitz-structured channel convolution, we derive an HQS-based alternating optimization to disentangle and estimate both the channel taps and nonlinear coefficients. Incorporating a DSP via an untrained 1D U-Net with TV regularization further stabilizes coefficient recovery. Experiments on real-world LoRa data demonstrate that our method maintains over 96.80%/91.19% in LOS/NLOS environments across unseen PA modules.

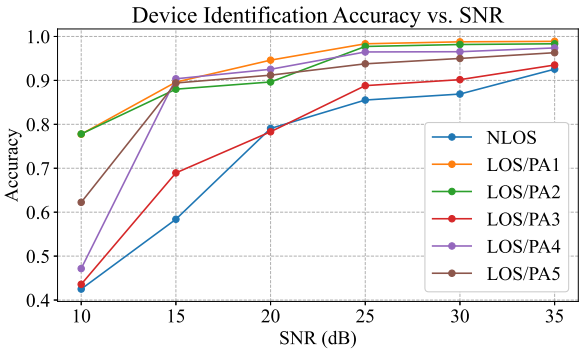

Fig. 3: Device classification accuracy under varying SNR conditions.

References

[1] J. Zhang, X. Zheng, Q. Liu, and R. Lin. "Radio Frequency Fingerprint Identification of GMSK Modulated Signals Based on Eye Diagram Traces Deviation," *IEEE Transactions on Vehicular Technology*, doi: 10.1109/TVT.2025.3543481.

[2] R. Kong and H. Chen. "DeepCRF: Deep Learning-Enhanced CSI-Based RF Fingerprinting for Channel-Resilient WiFi Device Identification," *IEEE Transactions on Information Forensics and Security*, vol. 20, pp. 264–278, 2025, doi: 10.1109/TIFS.2024.3515796.

[3] T. Ding, L. Peng, Y. Qiu, Z. Wu, and H. Fu. "A Research of I/Q Imbalance Based RF Fingerprint Identification with LTE-RACH Signals," in *Proceedings of the IEEE 6th International Conference on Signal and Image Processing (ICSIP)*, Nanjing, China, pp. 66–71, 2021, doi: 10.1109/ICSIP52628.2021.9688945.

[4] W. Hou, X. Wang, J.-Y. Chouinard, and A. Refaey. "Physical layer authentication for mobile systems with time-varying carrier frequency offsets," *IEEE Transactions on Communications*, vol. 62, no. 5, pp. 1658–1667, 2014.

[5] G. Huang, Y. Yuan, X. Wang, and Z. Huang. "Specific emitter identification based on nonlinear dynamical characteristics," *Canadian Journal of Electrical and Computer Engineering*, vol. 39, no. 1, pp. 34–41, 2016.

[6] Y. Li, Y. Ding, G. Goussetis, and S. K. Podilchak. "PUF-Assisted Radio Frequency Fingerprinting Exploiting Power Amplifier Active Load-Pulling," *IEEE Transactions on Information Forensics and Security*, vol. 19, pp. 5015–5029, 2024, doi: 10.1109/TIFS.2024.3389570.

[7] Y. Li, Y. Ding, J. Zhang, G. Goussetis, and S. K. Podilchak. "Radio frequency fingerprinting exploiting non-linear memory effect," *IEEE Transactions on Cognitive Communications and Networking*, vol. 8, no. 4, pp. 1618–1631, 2022.

[8] V. Chen, J. Xu, Y. Shen, and E. Chen. "RF fingerprint classification with combinatorial-randomness-based power amplifiers and convolutional neural networks: Secure analog/RF electronics and electromagnetics," *IEEE Solid-State Circuits Magazine*, vol. 14, no. 4, pp. 28–36, 2022.

[9] H. Fu, Y. Sun, L. Peng, and M. Liu. "Channel-Resilient RF Fingerprint Identification Based on Nonlinear Features With Memory Effect," *IEEE Communications Letters*, vol. 28, no. 4, pp. 798–802, 2024, doi: 10.1109/LCOMM.2024.3364494.

[10] L. Yang, S. Camtepe, Y. Gao, V. Liu, and D. Jayalath. "On the Use of Power Amplifier Nonlinearity Quotient to Improve Radio Frequency Fingerprint Identification in Time-Varying Channels," in *Proceedings of the IEEE 34th Annual International Symposium on Personal, Indoor and Mobile Radio Communications (PIMRC)*, Toronto, Canada, pp. 1–7, 2023, doi: 10.1109/PIMRC56721.2023.10293946.

[11] G. Zhang, Y. Lu, M. Li, Z. Zhong, and T. Q. S. Quek. "Joint Uplink and Downlink Robust Transmission for Cell-Free Networks," *IEEE Transactions on Wireless Communications*, vol. 23, no. 10, pp. 15308–15321, 2024, doi: 10.1109/TWC.2024.3428486.

[12] D. Ulyanov, A. Vedaldi, and V. Lempitsky. "Deep image prior," in *Proceedings of the IEEE Conference on Computer Vision and Pattern Recognition (CVPR)*, pp. 9446–9454, 2018.